Journal of Biomedical Optics

SPIEDigitalLibrary.org/jbo

Development of a stigmatic mass microscope using laser desorption/ionization and a multi-turn time-of-flight mass spectrometer

Hisanao Hazama
Hidetoshi Yoshimura
Jun Aoki
Hirofumi Nagao
Michisato Toyoda
Katsuyoshi Masuda
Kenichi Fujii
Toshio Tashima
Yasuhide Naito
Kunio Awazu

SPIE

Development of a stigmatic mass microscope using laser desorption/ionization and a multi-turn time-of-flight mass spectrometer

Hisanao Hazama,[a,g] Hidetoshi Yoshimura,[a,g] Jun Aoki,[b,g] Hirofumi Nagao,[c,g] Michisato Toyoda,[b,c,g] Katsuyoshi Masuda,[d,g] Kenichi Fujii,[e,g] Toshio Tashima,[g] Yasuhide Naito,[f,g] and Kunio Awazu[a,g]

[a]Osaka University, Graduate School of Engineering, 2-1 Yamadaoka, Suita, Osaka, 565-0871, Japan
[b]Osaka University, Graduate School of Science, 1-1 Machikaneyama, Toyonaka, Osaka, 560-0043, Japan
[c]Osaka University, Renovation Center of Instruments for Science Education and Technology, 1-2 Machikaneyama, Toyonaka, Osaka, 560-0043, Japan
[d]Suntory Institute for Bioorganic Research, 1-1-1 Wakayamadai, Shimamotocho, Mishimagun, Osaka, 618-8503, Japan
[e]Faculty of Information Science and Technology, Osaka Institute of Technology, 1-79-1 Kitayama, Hirakata, Osaka, 573-0196, Japan
[f]The Graduate School for the Creation of New Photonics Industries, 1955-1 Kurematsucho, Nishiku, Hamamatsu, Shizuoka, 431-1202, Japan
[g]Japan Science and Technology Agency, CREST, 5 Sanbancho, Chiyodaku, Tokyo, Japan 102-0075

Abstract. A novel stigmatic mass microscope using laser desorption/ionization and a multi-turn time-of-flight mass spectrometer, MULTUM-IMG, has been developed. Stigmatic ion images of crystal violet masked by a fine square mesh grid with a 12.7 μm pitch as well as microdot patterns with a 5 μm dot diameter and a 10 μm pitch made with rhodamine B were clearly observed. The estimated spatial resolution was about 3 μm in the linear mode with a 20-fold ion optical magnification. Separating stigmatic ion images according to the time-of-flight, i.e., the mass-to-charge ratio of the ions was successfully demonstrated by a microdot pattern made with two different dyes, crystal violet and methylene blue. Stigmatic ion images of a microdot pattern made with crystal violet were observed after circulation in MULTUM-IMG, and the pattern of the ion image was maintained after ten cycles in MULTUM-IMG. A section of a mouse brain stained with crystal violet and methylene blue was observed in the linear mode, and the stigmatic total ion image of crystal violet and methylene blue agreed well with the optical microphotograph of the hippocampus for the same section. [DOI: 10.1117/1.3561091]

Keywords: imaging mass spectrometry; stigmatic mass microscope; matrix-assisted laser desorption/ionization; multi-turn time-of-flight mass spectrometer.

Paper 10419PRR received Jul. 23, 2010; revised manuscript received Feb. 8, 2011; accepted for publication Feb. 11, 2011; published online Apr. 1, 2011.

1 Introduction

To elucidate the mechanisms of diseases and to develop drugs, numerous fields including pathology, pharmacokinetics, and so on require analytical techniques to measure spatial distributions of biomolecules such as proteins, peptides, and drugs introduced in biological tissues at the cellular-scale. In recent years, imaging mass spectrometry (IMS) using matrix-assisted laser desorption/ionization (MALDI)[1,2] and time-of-flight mass spectrometry has been commonly used to simultaneously measure two- or three-dimensional spatial distributions of multiple biomolecules or drugs and their metabolites without labeling target molecules.[3–11] In other analytical techniques using labels, only targeted molecules are observed. In addition to the targeted molecules, IMS can detect many kinds of unpredictable molecules and can identify them according to the mass-to-charge ratio of the ions.

MALDI-IMS is generally performed by scanning a laser spot on the sample surface because conventional instruments for MALDI mass spectrometry can be used with minimal modifications. However, the spatial resolution of MALDI-IMS is limited to about 10–100 μm due to the laser focus diameter, and measurements require a few to tens of hours. On the other hand, stigmatic (or microscope mode) IMS has recently been proposed.[7–9] In this technique, the entire sample is irradiated by a laser with a uniform intensity profile. Then the spatial distributions of the ions produced at the sample surface are magnified and projected onto a position- and time-sensitive ion detector. In stigmatic IMS, the spatial resolution is not restricted by the laser focus diameter. Thus cellular-scale observations and short time measurements should be possible. However, commercial instruments for stigmatic IMS are currently unavailable because many technical issues must be solved, e.g., the development of a position- and time-sensitive ion detector. Therefore, we are developing a novel stigmatic MALDI mass microscope for cellular-scale observations of biological samples. To obtain a high mass resolution necessary to analyze complex mixtures

Address all correspondence to: Hisanao Hazama, Osaka University, Graduate School of Engineering, Building #A14 2-1 Yamadaoka, Suita, Osaka, 565-0871 Japan. Tel: 81 6 6879-4735; Fax: 81 6 6879-7363; E-mail: hazama@wakate.frc.eng.osaka-u.ac.jp.

1083-3668/2011/16(4)/046007/7/$25.00

obtained from biological samples, we have adopted a multi-turn time-of-flight mass spectrometer,[12,13] which has been developed at Osaka University for the stigmatic mass microscope. The ion optical system used in the multi-turn time-of-flight mass spectrometer theoretically satisfies the perfect spatial and temporal focusing condition, i.e., in theory, the spatial distributions and the temporal deviations of ions prior to circulation of the multi-turn circuit are exactly reproduced after circulation, and the mass resolution is increased with increasing the number of circulation. The temporal focusing ability has already been demonstrated in previous experiments,[7,12,13] e.g., we have demonstrated an extremely high mass resolving power $m/\Delta m$ of 130,000 for ions of a peptide, angiotensin II (m/z 1046.5), after 500 cycles in the multi-turn time-of-flight mass spectrometer,[7] where m and Δm denote the mass number and the full width at half maximum of the peak of the ions on the mass spectrum, respectively. However, the spatial focusing ability of the multi-turn time-of-flight mass spectrometer has never been experimentally verified. Herein, the performance of the stigmatic mass microscope coupled with the multi-turn time-of-flight mass spectrometer is evaluated using both artificial patterns and a biological tissue section.

2 Experimental Apparatus

Figure 1 schematically depicts the stigmatic mass microscope equipped with a MALDI ion source and a multi-turn time-of-flight mass spectrometer, MULTUM-IMG. The third harmonic wave of a Q-switched Nd:YAG laser (SLMQ1S-10, Spectron Laser Systems Ltd., Warwickshire, England) was introduced into the MALDI ion source and focused onto the sample plate at a diameter of about 0.8 mm, incident angle of 20 deg, and repetition rate of 10 Hz. Ions produced at the sample plate surface were accelerated at the ion source. The produced ion spatial distributions, which were magnified and projected with an einzel lens and a quadrupole triplet lens onto a chevron-stacked dual microchannel plate (MCP) and phosphor screen assembly (F2223-21PGFX, Hamamatsu Photonics K. K., Shizuoka, Japan), were recorded with a camera lens (MLM-3XMP, CBC Co., Ltd., Tokyo, Japan) and a cooled charge-coupled device (CCD) camera (CoolSNAP HQ^2, Roper Scientific, Inc., Tucson, AZ, USA). The time-of-flight spectra of the ions spatially averaged over the MCP surface were recorded with a high-frequency decoupler connected to the MCP and a digital oscilloscope (WaveMaster 8600A, LeCroy, Chestnut Ridge, NY, USA).

The acceleration region at the ion source consisted of a sample plate, extraction electrode, and ground electrode. Both the extraction and ground electrodes had circular apertures with 4 mm diameters. The separation between the sample plate and the extraction electrode was 2.5 mm, while that of the extraction and ground electrodes was 17 mm. An acceleration voltage of up to 20 kV was statically applied to the sample plate, and the ground electrode was connected to the ground. The voltage of the extraction electrode was statically set to 96% of the acceleration voltage.

MULTUM-IMG has four sector electrodes that produce a figure-eight ion trajectory. In each sector, toroidal electric field was produced by a combination of cylindrical electric condenser and a pair of plane electrodes called Matsuda plates.[14] When ions were introduced from the MALDI ion source to the multi-turn portion of MULTUM-IMG, the voltage to sector I was turned on while that to sector IV was turned off. The voltages to sectors II and III were statically applied throughout the experiments. After the ions were introduced into the multi-turn circuit, the voltage to sector IV was turned on. The number of cycles in the multi-turn circuit was controlled by adjusting the time when the voltage to sector I was turned off. MULTUM-IMG could also be used as a linear time-of-flight mass spectrometer (linear mode) by turning off the voltages to both sectors I and IV. A deflector adjacent to sector IV was used as an ion gate to select ions according to the time-of-flight by adjusting the time when the high voltage pulse was applied to the deflector.

The linear flight path length from the sample plate to the MCP was 0.96 m, and the path length in the multi-turn circuit per unit cycle was 1.308 m. In some experiments, the linear flight path length was extended to 1.46 m to enhance the ion optical magnification. The background pressures at the ion source and

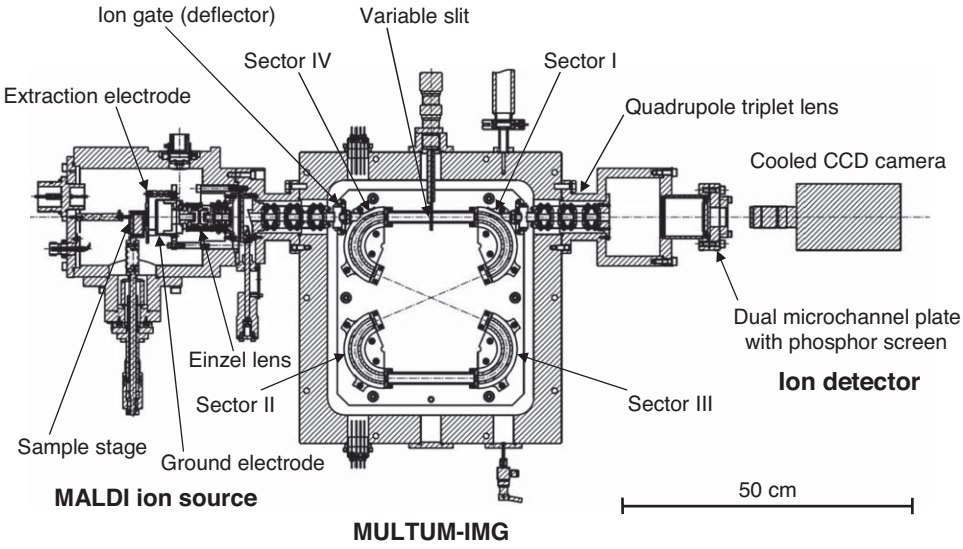

Fig. 1 Schematic drawing of the experimental apparatus for stigmatic imaging mass spectrometry.

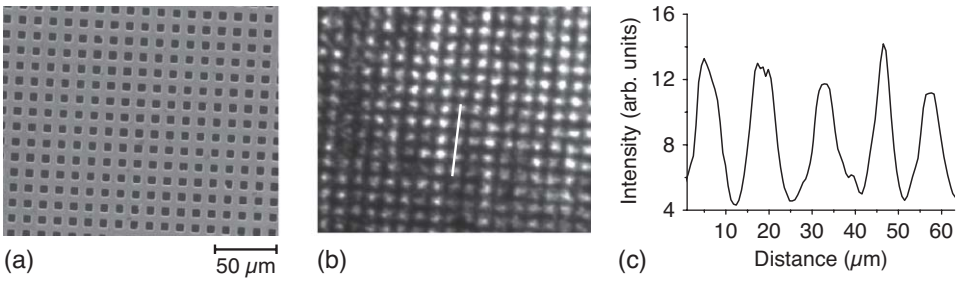

Fig. 2 (a) Fine square mesh grid with a 12.7 μm pitch observed using a scanning electron microscope, (b) stigmatic ion image of a dried droplet of a crystal violet solution covered by the grid, and (c) ion signal intensity profile along the line drawn in the ion image. Ion image was observed in the linear mode with an extended flight path length of 1.46 m at an acceleration voltage of 20 kV and a CCD exposure time of 10 s (100 laser shots) without using a quadrupole triplet lens.

MULTUM-IMG were about 3×10^{-5} Pa. A digital delay/pulse generator (Model 555, Berkeley Nucleonics, Richmond, CA, USA) was used to generate the timing signals for the Nd:YAG laser, the voltage pulses for sectors I and IV, the ion gate, and the digital oscilloscope.

3 Sample Preparation

3.1 *Artificial Patterns*

To evaluate the performance of the stigmatic mass microscope, artificial patterns were made with dyes capable of ionization without a matrix, i.e., by "direct" laser desorption/ionization. An aqueous solution of crystal violet with a volume of 2 μL was dropped on a stainless steel sample plate. The dried droplet of the crystal violet was masked by a fine square mesh grid composed of nickel (G2000HS, Gilder Grids, Lincolnshire, England). The pitch and bar width of the mesh were 12.7 and 5 μm, respectively, and this mesh was the finest commercial mesh available to us.

Microdot patterns were created by depositing microdroplets of dye solutions at a diameter of 5–100 μm and a constant pitch of 10–150 μm onto a slide glass with a conductive and transparent coating using indium tin oxide (ITO). Microdroplets of aqueous solution of rhodamine B with a diameter of 5 μm and a pitch of 10 μm were deposited using an on-demand droplet spotter.[15,16] On the other hand, microdroplets of aqueous solutions of crystal violet (CV) and methylene blue (MB) with a diameter of 15–100 μm and a pitch of 15–150 μm were deposited via the contact depositing technique.[17]

3.2 *Biological Sample*

A brain of a mouse (C57BL/6J, 6 weeks old) was extracted under anesthesia with diethyl ether. The extracted brain was immediately frozen with powdery dry ice and stored at -80°C. The brain was sliced into a thickness of 10 μm using a cryostat microtome (CM1850, Leica Microsystems, Wetzlar, Germany) at a temperature of -20°C and attached onto a slide glass coated with ITO. A section of the brain was stained with a solution of CV and MB dissolved in 70% aqueous ethanol at a concentration of 0.5 wt. % for each dye and subsequently washed with distilled water. The double staining method using CV and MB has recently been developed for endocytoscopy in gastroenterological endoscopy,[18] and CV and MB chiefly stain the cytoplasm and nucleus, respectively. The stained section of the brain was coated by an 8 nm thick layer of gold using an ion beam sputtering system (E-1010, Hitachi High-Technologies Corp., Tokyo, Japan). This study was approved by the Institutional Animal Experiments Committee and conducted in accordance with the guidelines of animal experimentation at Osaka University.

4 Results and discussion

4.1 *Stigmatic Ion Images of Artificial Patterns Observed in the Linear Mode*

Figure 2 shows the fine square mesh grid observed with a scanning electron microscope (JCM-5700, JEOL Ltd., Tokyo, Japan) and a stigmatic ion image of the pattern made with the mesh observed in the linear mode. In this case, positive ions produced by the detachment of Cl^- from crystal violet, $[CV–Cl]^+$, were detected. The ion optical magnification was about 20-fold, and the mesh pattern was clearly formed. The spatial resolution was estimated by the definition used by Colliver et al.[19] and Luxemburg et al.,[8] i.e., the spatial resolution was defined as the distance along the ion signal intensity profile for which the intensity increased from 20 to 80% of the maximum intensity. This definition was adopted to evaluate the spatial resolution in the micrometer range using the mesh with the pitch of 12.7 μm. The spatial resolution estimated from the ion signal intensity profile shown in Fig. 2(c) was about 3 μm. Additionally, a stigmatic ion image of the microdot pattern made with rhodamine B was observed. Figure 3 confirms that the ion image of the

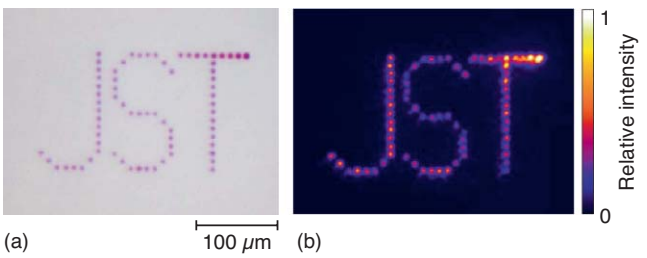

Fig. 3 (a) Optical microphotograph of a microdot pattern made with rhodamine B and (b) stigmatic ion image of the microdot pattern. Diameter and pitch of the dots were 5 and 10 μm, respectively. Ion image was observed in the linear mode at an acceleration voltage of 5 kV and a CCD exposure time of 10 s (100 laser shots) without using a quadrupole triplet lens.

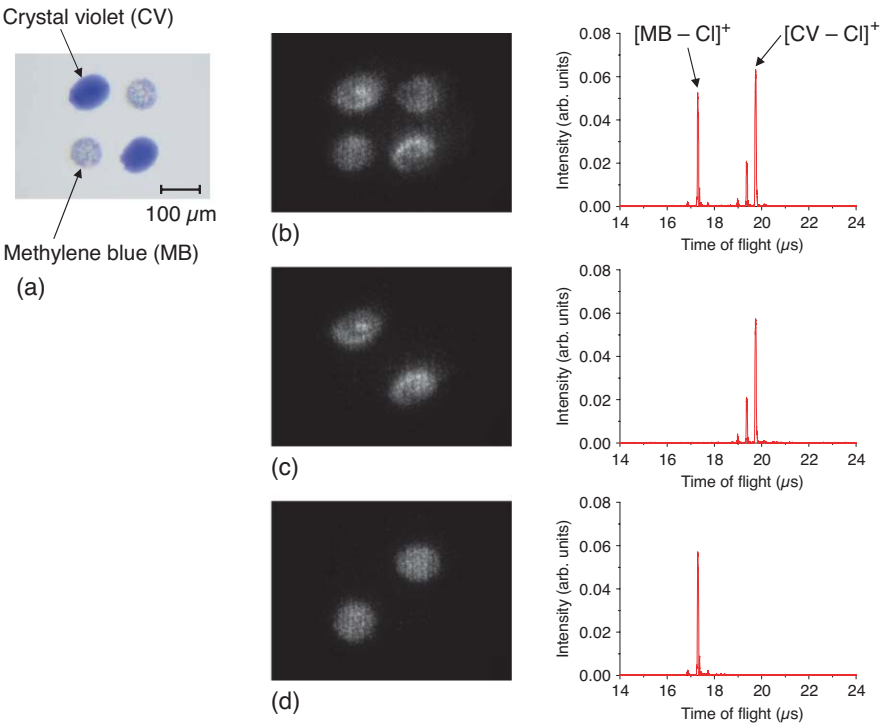

Fig. 4 (a) Optical microphotograph of a microdot pattern made with crystal violet (CV) and methylene blue (MB), and (b) stigmatic ion images and their corresponding time-of-flight spectra of the microdot pattern where ions originating from both CV and MB, (c) CV only, and (d) MB only were able to pass through the ion gate. $[CV–Cl]^+$ and $[MB–Cl]^+$ indicate singly charged positive ions produced by the detachment of Cl^- from CV and MB, respectively. All ion images were observed in the linear mode at an acceleration voltage of 5 kV and a CCD exposure time of 1 s (10 laser shots) without using a quadrupole triplet lens. The time-of-flight spectra were averaged over 10 s (100 laser shots).

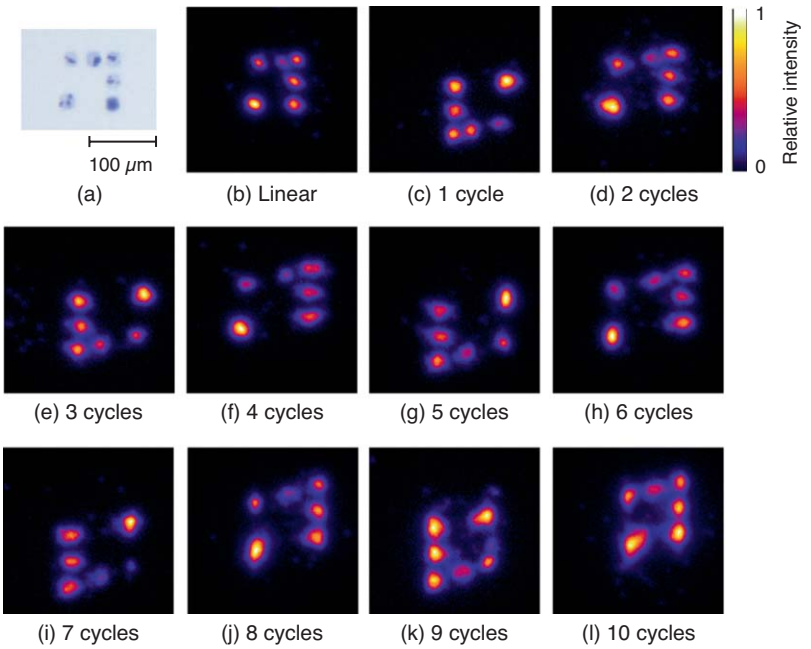

Fig. 5 (a) Optical microphotograph of a microdot pattern made with CV and (b) stigmatic ion images of the pattern obtained in the linear mode, and (c)–(l) after circulation in the MULTUM-IMG. All ion images were observed at an acceleration voltage of 5 kV and a CCD exposure time of 5 s (50 laser shots) using a quadrupole triplet lens.

microdot pattern agreed well with the optical microphotograph of the pattern, and dots with a diameter of 5 μm and a pitch of 10 μm were clearly resolved.

Figure 4 shows the stigmatic ion images and the corresponding time-of-flight spectra of the microdot pattern made with CV and MB. When both CV and MB ions passed through the ion gate, both were observed in the ion image and the time-of-flight spectrum. On the other hand, when only CV (or MB) ions were selected using the ion gate, the ion image and the time-of-flight spectrum contained only CV (or MB) ions. Hence, separation of stigmatic ion images according to the time-of-flight, i.e., the mass-to-charge ratio of the ions, was successful.

4.2 *Stigmatic Ion Images of Microdot Patterns Observed after Circulation in MULTUM-IMG*

Figure 5 shows stigmatic ion images measured in the linear mode and after circulation in the multi-turn circuit of MULTUM-IMG. As shown in Fig. 5(b), the ion image of the microdot pattern made with CV was clearly observed in the linear mode. In this case, a quadrupole triplet lens was used and the ion optical magnification was about 10-fold. Although slightly distorted, the ion images were maintained after circulation in MULTUM-IMG, as shown in Figs. 5(c)–5(l). Because the magnification of the ion optical system of the multi-turn circuit in MULTUM-IMG is -1, the four directions of the ion image were reversed for every cycle in MULTUM-IMG. The mass resolving power $m/\Delta m$ for $[CV–Cl]^+$ ion (m/z 372.2) was 150 in the linear mode and was increased to 2,000 after ten cycles in MULTUM-IMG.

With an acceleration voltage of 5 kV, the voltages to the outer and inner cylindrical sector electrodes were theoretically 1 kV and -1 kV, respectively. However, ion images were not observed after circulation in MULTUM-IMG by applying the theoretical voltages to the sector electrodes. Thus, the voltage applied to each sector electrode was individually optimized to minimize distortion in the ion images after circulation in MULTUM-IMG, and the maximum discrepancy between the theoretical and optimized voltages was about 10%. From the calculation results obtained with an in-house built three-dimensional simulation code using the surface-charge method,[20] it was hypothesized that the discrepancy between the theoretical and optimized voltages was due to the insufficient precision of the alignment between the electrodes in the ion source and MULTUM-IMG.

4.3 *Observations of Tissue Sections Stained with Dyes in the Linear Mode*

Stigmatic total ion images of the ions of CV and MB produced from the stained section of the brain were observed in the linear mode at a 20-fold ion optical magnification and were compared to an optical microphotograph of the section (Fig. 6). As shown in Fig. 6(c), the CV and MB ions produced by detachment of Cl^- were detected, but not ions originating in biomolecules such as lipids, peptides, and proteins. Because the field of view for a single measurement was a circular area with a diameter of about 400 μm, 78 ($=13\times6$) stigmatic ion images were recorded by moving the sample stage at a constant pitch of 250 μm. These images were combined using in-house software without compensation.

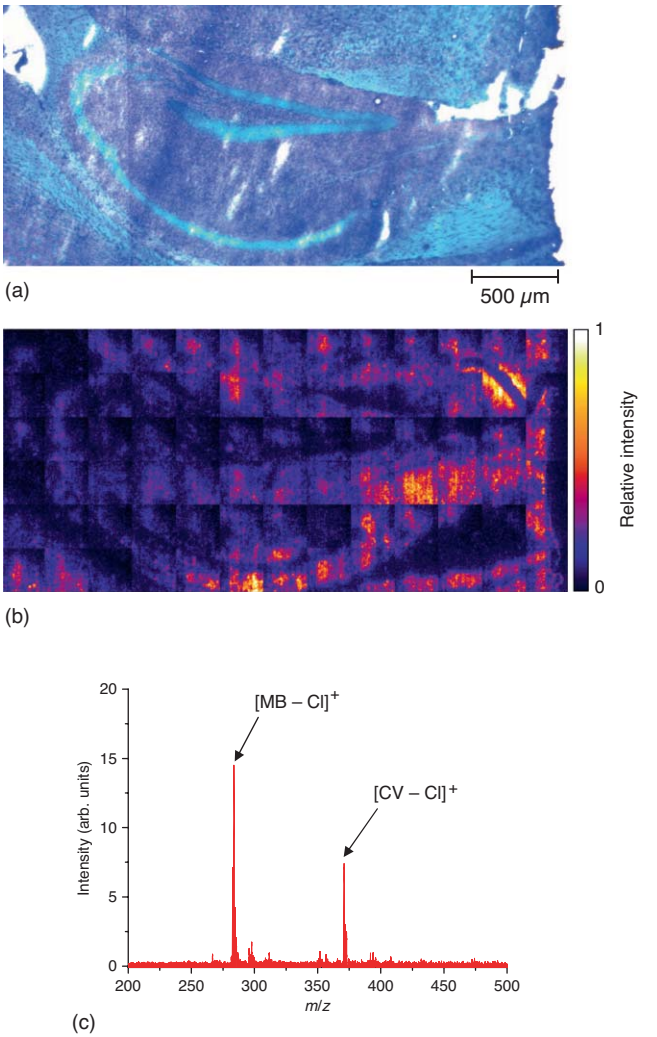

Fig. 6 (a) Optical microphotograph of the hippocampus in a section of a mouse brain stained with CV and MB, (b) stigmatic total ion image of the hippocampus obtained by combining 78 stigmatic total ion images, and (c) typical mass spectrum obtained from the hippocampus. Each ion image was observed in the linear mode with an extended flight path length of 1.46 m at an acceleration voltage of 20 kV and a CCD exposure time of 10 s (100 laser shots) without using a quadrupole triplet lens. The mass spectrum was averaged over 10 s.

The ion image of the dyes on the hippocampus in the brain for an area measuring 3.25 mm $\times$ 1.5 mm agreed well with the optical microphotograph of the same part of the sample. Not coating the section of brain with gold resulted in the ion image being undetectable. In this case, it was assumed that the ion image was disturbed by the change in the sample potential due to charge accumulation on the sample surface.[9] Ion images for CV only and MB only did not significantly differ. Each stigmatic total ion image was recorded with an exposure time of 10 s (100 laser shots), so that 78 stigmatic ion images can be collected within about 13 min. Although the repetition rate of the flashlamp-pumped Nd:YAG laser used in this study is 10 Hz, diode-pumped solid-state lasers with a repetition rate higher than 1 kHz have been available in recent years. Consequently, the total measurement time for 78 stigmatic ion images could be reduced to about 10 s using a laser with a 1 kHz repetition rate and automation of measurements. On the other hand, the

estimated time required for a measurement for the same area of 3.25 mm × 1.5 mm using a state of the art instrument for scanning imaging mass spectrometry is about 1.4 h, where the pitch of the scan, number of laser shots for each spot, and repetition rate of laser pulses are assumed to be 10 μm, 100 shots, and 1 kHz, respectively.[10,11] Therefore, it is suggested that the stigmatic mass microscope developed in this research is suitable for high-spatial resolution and high-throughput imaging mass spectrometry.

5 Conclusion

A stigmatic mass microscope has been developed using a MALDI ion source, a multi-turn time-of-flight mass spectrometer, MULTUM-IMG, and an MCP and phosphor screen detector assembly. Ion images of crystal violet masked with a fine square mesh grid with a pitch of 12.7 μm and a microdot pattern of rhodamine B with a diameter of 5 μm and a pitch of 10 μm were successfully observed in the linear mode. The estimated spatial resolution was about 3 μm. Moreover, stigmatic ion images were successfully separated according to the mass-to-charge ratio using the microdot pattern made with CV and MB. Additionally, stigmatic ion images after circulation in MULTUM-IMG of the microdot pattern made with CV was observed, and conservation of the ion image of the sample after circulation in MULTUM-IMG was experimentally demonstrated for the first time. The mass resolving power $m/\Delta m$ of 150 for $[\mathrm{CV–Cl}]^+$ ion (m/z 372.2) in the linear mode was increased to 2,000 after ten cycles in MULTUM-IMG. Furthermore, the stigmatic ion image of hippocampus in a section of a mouse brain stained with CV and MB observed in the linear mode agreed well with the optical microphotograph of the same part of the section. The stigmatic mass microscope developed in this research should be suitable for high-spatial resolution and high-throughput imaging mass spectrometry.

As the next step, observations of ion images of biomolecules such as lipids, peptides, proteins, and drugs introduced into tissues will be performed using MALDI. Because the ion detection system used in this experiment can measure only the total ion image or the ion image selected by the ion gate, we are currently developing a position- and time-sensitive ion detection system using a delay-line detector.[21–24]

Acknowledgments

We thank Masahiro Hayashi, Shuichi Shimma, and Shu Taira for their helpful suggestions and Toshio Ichihara for his technical support. This work was supported by the Japan Science and Technology Agency, Core Research for Evolutional Science and Technology (CREST). The authors gratefully appreciate the advisory board of CREST, Michiyoshi Tanaka, Koji Kuroda, Makoto Sakai, and Itsuo Katakuse for their helpful discussions.

References

1. M. Karas and F. Hillenkamp, "Laser desorption ionization of proteins with molecular masses exceeding 10000 daltons," *Anal. Chem.* **60**(20), 2299–2301 (1988).
2. M. Mann, R. C. Hendrickson, and A. Randy, "Analysis of proteins and proteomes by mass spectrometry," *Annu. Rev. Biochem.* **70**, 437–473 (2001).
3. S. S. Rubakhin, J. C. Jurchen, E. B. Monroe, and J. V. Sweedler, "Imaging mass spectrometry: fundamentals and applications to drug discovery," *Drug Discovery Today* **10**(12), 823–837 (2005).
4. S. Khatib-Shahidi, M. Andersson, J. L. Herman, T. A. Gillespie, and R. M. Caprioli, "Direct molecular analysis of whole-body animal tissue sections by imaging MALDI mass spectrometry," *Anal. Chem.* **78**(18), 6448–6456 (2006).
5. M. Andersson, M. R. Groseclose, A. Y. Deutch, and R. M. Caprioli, "Imaging mass spectrometry of proteins and peptides: 3D volume reconstruction," *Nat. Methods* **5**(1), 101–108 (2008).
6. T. Harada, A. Yuba-Kubo, Y. Sugiura, N. Zaima, T. Hayasaka, N. Goto-Inoue, M. Wakui, M. Suematsu, K. Takeshita, K. Ogawa, Y. Yoshida, and M. Setou, "Visualization of volatile substances in different organelles with an atmospheric-pressure mass microscope," *Anal. Chem.* **81**(21), 9153–9157 (2009).
7. H. Hazama, J. Aoki, H. Nagao, R. Suzuki, T. Tashima, K. Fujii, K. Masuda, K. Awazu, M. Toyoda, and Y. Naito, "Construction of a novel stigmatic MALDI imaging mass spectrometer," *Appl. Surf. Sci.* **255**(4), 1257–1263 (2008).
8. S. L. Luxemburg, T. H. Mize, L. A. McDonnell, and R. M. A. Heeren, "High-spatial resolution mass spectrometric imaging of peptide and protein distributions on a surface," *Anal. Chem.* **76**(18), 5339–5344 (2004).
9. A. F. M. Altelaar, I. Klinkert, K. Jalink, R. P. J. de Lange, R. A. H. Adan, R. M. A. Heeren, and S. R. Piersma, "Gold-enhanced biomolecular surface imaging of cells and tissue by SIMS and MALDI mass spectrometry," *Anal. Chem.* **78**(3), 734–742 (2006).
10. L. A. McDonnell and R. M. A. Heeren, "Imaging mass spectrometry," *Mass Spectrom. Rev.* **26**(4), 606–643 (2007).
11. K. Chughtai and R. M. A. Heeren, "Mass spectrometric imaging for biomedical tissue analysis," *Chem. Rev.* **110**(5), 3237–3277 (2010).
12. M. Toyoda, D. Okumura, M. Ishihara, and I. Katakuse, "Multi-turn time-of-flight mass spectrometers with electrostatic sectors," *J. Mass Spectrom.* **38**(11), 1125–1142 (2003).
13. M. Toyoda, "Development of multi-turn time-of-flight mass spectrometers and their applications," *Eur. J. Mass Spectrom.* **16**(3), 397–406 (2010).
14. H. Matsuda and Y. Fujita, "Potential distribution in a cylindrical condenser terminated by Matsuda plates," *Int. J. Mass Spectrom. Ion Phys.* **16**(4), 395–404 (1975).
15. O. Yogi, T. Kawakami, M. Yamauchi, J. Y. Ye, and M. Ishikawa, "On-demand droplet spotter for preparing pico- to femtoliter droplets on surfaces," *Anal. Chem.* **73**(8), 1896–1902 (2001).
16. O. Yogi, T. Kawakami, and A. Mizuno, "Properties of droplet formation made by cone jet using a novel capillary with an external electrode," *J. Electrost.* **64**(7–9), 634–638 (2006).
17. T. Tashima, M. Toyoda, H. Hazama, K. Fujii, J. Aoki, K. Masuda, K. Awazu, and Y. Naito, "Preparation of micro-dot patterns used to evaluate spatial resolution of stigmatic mass spectrometric microscope with multi-turn TOF," *Abstracts 57th Annu. Conf. Mass Spectrom. Jpn.*, 176–177 (2009).
18. H. Inoue, M. Kaga, H. Minami, S. Sugaya, Y. Sato, K. Sasajima, S. Hamatani, A. Shiokawa, and S. Kudo, "Ultra-high magnifying endoscopy; from endomicroscopy to endocytoscopy (in Japanese)," *Gastroenterol. Endosc.* **49**(11), 2811–2818 (2007).
19. T. L. Colliver, C. L. Brummel, M. L. Pacholski, F. D. Swanek, A. G. Ewing, and N. Winograd, "Atomic and molecular imaging at the single-cell level with TOF-SIMS," *Anal. Chem.* **69**(13), 2225–2231 (1997).
20. J. Aoki, A. Kubo, M. Ishihara, and M. Toyoda, "Simulation of ion trajectories using the surface-charge method on a special purpose computer," *Nucl. Instrum. Methods Phys. Res. A* **600**(2), 466–470 (2009).
21. A. Oelsner, O. Schmidt, M. Schicketanz, M. Klais, G. Schönhense, V. Mergel, O. Jagutzki, and H. Schmidt-Böcking, "Microspectroscopy and imaging using a delay line detector in time-of-flight photoemission microscopy," *Rev. Sci. Instrum.* **72**(10), 3968–3974 (2001).

22. O. Jagutzki, A. Cerezo, A. Czasch, R. Dörner, M. Hattaß, M. Huang, V. Mergel, U. Spillmann, K. Ullmann-Pfleger, T. Weber, H. Schmidt-Böcking, and G. D. W. Smith, "Multiple hit readout of a microchannel plate detector with a three-layer delay-line anode," *IEEE Trans. Nucl. Sci.* **49**(5), 2477–2483 (2002).
23. G. D. Costa, F. Vurpillot, A. Bostel, M. Bouet, and B. Deconihout, "Design of a delay-line position-sensitive detector with improved performance," *Rev. Sci. Instrum.* **76**(1), 013304 (2005).
24. A. Czasch, J. Milnes, N. Hay, W. Wicking, and O. Jagutzki, "Position- and time-sensitive single photon detector with delay-line readout," *Nucl. Instrum. Methods Phys. Res. A* **580**(2), 1066–1070 (2007).